An Efficient Method for the Computation of Legendre Moments

Pew-Thian Yap and
Raveendran Paramesran, *Member, IEEE*

Abstract—Legendre moments are continuous moments, hence, when applied to discrete-space images, numerical approximation is involved and error occurs. This paper proposes a method to compute the exact values of the moments by mathematically integrating the Legendre polynomials over the corresponding intervals of the image pixels. Experimental results show that the values obtained match those calculated theoretically, and the image reconstructed from these moments have lower error than that of the conventional methods for the same order. Although the same set of exact Legendre moments can be obtained indirectly from the set of geometric moments, the computation time taken is much longer than the proposed method.

Index Terms—Moments, feature representation.

---- ✦ ----

1   INTRODUCTION

THE set of Legendre moments was introduced by Teague [1] as a set of orthogonal moments for image analysis. Examples of applications of Legendre moments include pattern recognition [2], image indexing [3], face recognition [4], and line fitting [5]. However, when applied to discrete-space images, the set of Legendre polynomials [6], [7], [8], which forms the kernel of the Legendre moments, is approximated by sampling at fixed intervals. Hence, the Legendre moments generated have approximated values and do not match those obtained theoretically. Moreover, the error due to approximation generally increases as the order of the moments is increased [9].

Previously, Liao and Pawlak [9], [10], [11] performed an error analysis on the set of Legendre moments and proposed to use the alternative extended Simpson's rule (AESR) to minimize the error. However, the moments computed, while small in error, is not exact. Some other works on Legendre moments can be found in [12], [11], [10], [9], [8], [7], [6], [5], [4], [3], [2].

This paper proposes an algorithm for the exact computation of the set of Legendre moments. This is done by mathematically integrating the Legendre polynomials over the corresponding intervals of the image pixels when mapped into $[-1, 1] \times [-1, 1]$. It is shown that the method gives exact values when compared to those obtained by theoretical calculations. Experimental results show that the images reconstructed from the set of Legendre moments calculated using the proposed method have lower errors when compared to the that using zeroth-order approximation (ZOA) or AESR. This is especially the case when considering the fact that the later methods are susceptible to undersampling (discussed in Section 3). Though there is an increase in the computation time using the proposed method, it is marginal and the difference in computation time between the proposed and the conventional methods can be avoided by precomputing and storing the related kernel.

• *The authors are with the Department of Electrical Engineering, University of Malaya, 50603 Kuala Lumpur, Malaysia.*
  E-mail: ptyap@time.net.my, ravee@um.edu.my.

Legendre moments can be expressed as the linear combinations of geometric moments [18]. Hence, it can be shown that by first computing the exact values of the set of geometric moments and then combining them linearly, the set of exact Legendre moments can be formulated. However, though the exact values can be obtained using this method, the computation time to derive them is much longer than the method proposed in this paper. The experimental validation for this point will be given later in this paper.

The rest of this paper is organized as follows: Section 2 gives an theoretical overview of Legendre moments. Section 3 discusses the effects of approximation on Legendre moments. In Section 4, we propose a method to compute the set Legendre moments exactly. Section 5 gives the experimental validation of the theoretical framework. Section 6 concludes this paper.

2   LEGENDRE MOMENTS

Legendre moments of order $(m + n)$ are defined as:

$$\lambda_{mn} = \frac{(2m + 1)(2n + 1)}{4} \int_{-1}^{1} \int_{-1}^{1} P_m(x) P_n(y) f(x, y) dx dy, \quad (1)$$

where $m, n = 1, 2, 3, \ldots \infty$. The nth-order Legendre polynomials are defined as:

$$P_n(x) = \sum_{k=0}^{n} a_{k,n} x^k = \frac{(-1)^n}{2^n n!} \left(\frac{d}{dx} \right)^n \left[(1 - x^2)^n \right], \quad (2)$$

and can also be written as [19]:

$$\begin{aligned} P_n(x) &= \sum_{k=0}^{D(n)} (-1)^k \frac{(2n - 2k)!}{2^n k!(n - k)!(n - 2k)!} x^{n-2k} \\ &= \frac{(2n)!}{2^n (n!)^2} x^n - \frac{(2n - 2)!}{2^n 1!(n - 1)!(n - 2)!} x^{n-2} + \ldots, \end{aligned} \quad (3)$$

where $D(n) = n/2$ or $(n - 1)/2$, whichever is an integer. The set of Legendre polynomials $\{P_n(x)\}$ forms a complete orthogonal basis set on the interval $[-1, 1]$:

$$\int_{-1}^{1} P_n(x) P_m(x) dx = \frac{2}{2n + 1} \delta_{nm}. \quad (4)$$

For the computation of Legendre polynomials, the recurrence relation can be used:

$$(n + 1) P_{n+1}(x) - (2n + 1) x P_n(x) + n P_{n-1}(x) = 0. \quad (5)$$

A piece-wise continuous and bounded image function $f(x, y)$ can be written as an infinite series of expansion in terms of the Legendre polynomials over the square $[-1 \le x, y \le 1]$:

$$f(x, y) = \sum_{m=0}^{\infty} \sum_{n=0}^{\infty} \lambda_{mn} P_m(x) P_n(y), \quad (6)$$

where the Legendre moments $\{\lambda_{mn}\}$ are computed over the same square. If only Legendre moments of order $(m + n) \le L$ are given, then the function $f(x, y)$ can be approximated by a truncated finite series:

$$\hat{f}(x, y; L) = \sum_{m=0}^{L} \sum_{n=0}^{m} \lambda_{m-n,n} P_{m-n}(x) P_n(y). \quad (7)$$

If the Legendre moments are limited to those with $m \le m_{\max}$ and $n \le n_{\max}$, then the approximation becomes:

$$\hat{f}(x, y; m_{\max}, n_{\max}) = \sum_{m=0}^{m_{\max}} \sum_{n=0}^{n_{\max}} \lambda_{mn} P_m(x) P_n(y). \quad (8)$$
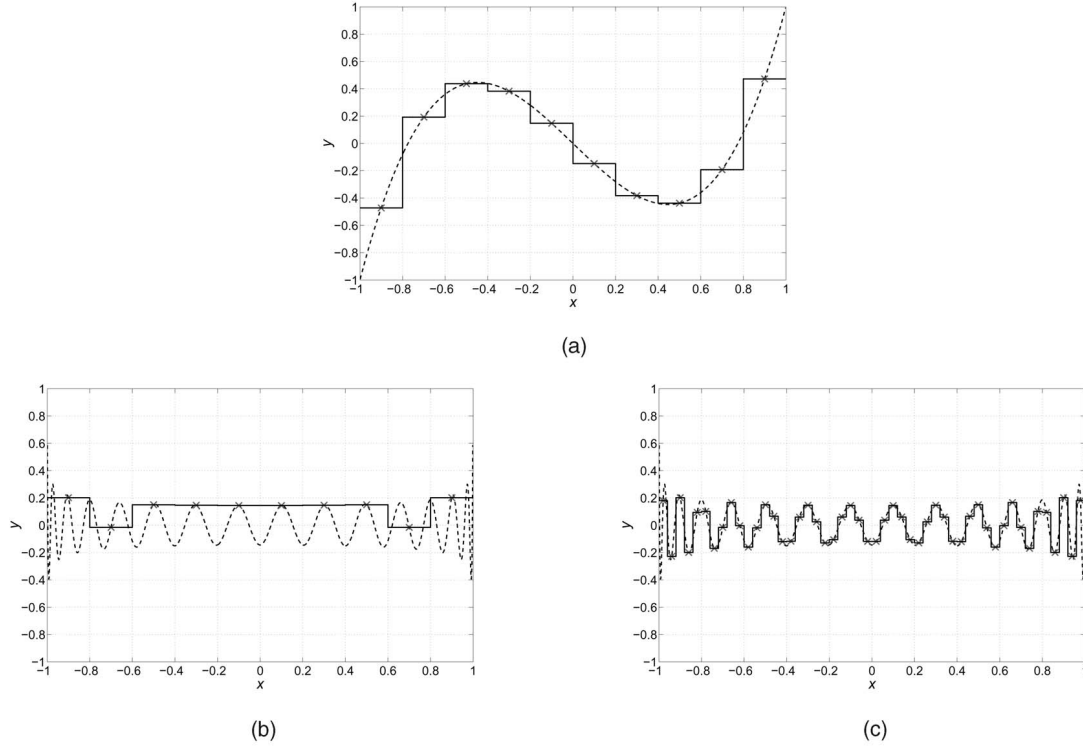
(a)

(b)

(c)

Fig. 1. The actual Legendre polynomials are shown by the dashed lines and the approximated ones by the solid lines. The approximated Legendre polynomials are obtained by sampling the actual Legendre polynomials at the middle point of each sampling interval as indicated by "×." (a) The third order Legendre polynomial sampled at 10 points. (b) The 30th order Legendre polynomial sampled at 10 points. (c) The 30th order Legendre polynomial sampled at 50 points.

3 APPROXIMATION ERROR

Considering a discrete-space image of size $M \times N$. $f(x,y)$ is defined only for a discrete set of points $(x_i, y_j) \in [-1,1] \times [-1,1]$, $i = 0, 1, \ldots, M-1$, $j = 0, 1, \ldots, N-1$. Hence, from (1), we have:

$$\lambda_{mn} = \frac{(2m+1)(2n+1)}{4} \sum_{i=0}^{M-1} \sum_{j=0}^{N-1} f(x_i, y_j)$$

$$\int_{x_i - \frac{\Delta x_i}{2}}^{x_i + \frac{\Delta x_i}{2}} \int_{y_j - \frac{\Delta y_j}{2}}^{y_j + \frac{\Delta y_j}{2}} P_m(x) P_n(y) dx dy, \quad (9)$$

where $\Delta x_i = x_{i+1} - x_i$ and $\Delta y_j = y_{j+1} - y_j$. The integral terms in (9) are often evaluated by zeroth-order approximation, that is, the values of Legendre polynomials are assumed to be constant over the intervals $\left[x_i - \frac{\Delta x_i}{2}, x_i + \frac{\Delta x_i}{2}\right]$ and $\left[y_j - \frac{\Delta y_j}{2}, y_j + \frac{\Delta y_j}{2}\right]$, and the values for each interval are obtained by sampling the Legendre polynomials at the central points of these intervals (see Fig. 1). In this case, the set of approximated Legendre moments is defined as:

$$\widehat{\lambda}_{mn} = \frac{(2m+1)(2n+1)}{MN} \sum_{i=0}^{M-1} \sum_{j=0}^{N-1} f(x_i, y_j) P_m(x_i) P_n(y_j). \quad (10)$$

This approximation of the integral terms causes error in the computed Legendre moments and the error can be obtained by:

$$E(\widehat{\lambda}_{mn}) = \lambda_{mn} - \widehat{\lambda}_{mn}$$

$$= \frac{(2m+1)(2n+1)}{4} \sum_{i=0}^{M-1} \sum_{j=0}^{N-1} f(x_i, y_j)$$

$$\left[\int_{x_i - \frac{\Delta x_i}{2}}^{x_i + \frac{\Delta x_i}{2}} \int_{y_j - \frac{\Delta y_j}{2}}^{y_j + \frac{\Delta y_j}{2}} P_m(x) P_n(y) dx dy - \frac{4}{MN} P_m(x_i) P_n(y_j) \right]. \quad (11)$$

It should be noted that this error increases as the number of sampling points decreases and increases further if the order of the moments is also increased [9]. This increase in error can be explained from the perspective of the sampling problem. Legendre polynomials are oscillating functions like sine and cosine functions. This can be observed from the fact that, for the nth order Legendre polynomial, all of the n zeros are real, distinct and are located inside the interval $[-1, 1]$ [8]. This implies that when the order is increased, the shape of the polynomial will oscillate at a higher spatial-frequency. This is verified by comparing the plots of the Legendre polynomials (dashed lines) as shown in Figs. 1a and 1b. Fig. 1a shows the graphical plot of the third order Legendre polynomial, where the curve crossed the line $y = 0$ at three points. Fig. 1b shows the Legendre polynomial of the 30th order, where the line $y = 0$ is crossed at 30 points. In this case, the curve is oscillating at a much higher frequency. Since the zeroth-order approximated Legendre moments are computed by first sampling the Legendre polynomials at discrete intervals, the moments are susceptible to information loss, especially if the Legendre polynomials are undersampled. Note that the number of sampling points are fixed by the size $M \times N$ of the image. Hence, when high-order moments are considered, the sampling of the Legendre polynomials becomes insufficient and hence undersampled. This can be observed by comparing Figs. 1b and 1c. In Fig. 1b, only 10 sampling points are used and, in Fig. 1c, 50 sampling points are used. In Fig. 1c, the approximated Legendre polynomial (solid line) matches the actual Legendre polynomial (dashed line) much better when compared to the case of Fig. 1b. We shall see in the next section that this problem can be remedied by computing the set of Legendre polynomials exactly by integrations over the pixel intervals.

4 EXACT COMPUTATION OF LEGENDRE MOMENTS

In the previous section, the approximation of the integrals in (9) is responsible for the approximation error of the Legendre moments.

We propose to remedy this by evaluating the integrals directly by using (3), that is:

$$\int_{x_i-\frac{\Delta x_i}{2}}^{x_i+\frac{\Delta x_i}{2}} P_m(x)dx = \sum_{r=0}^{D(m)} B_{rm} \left[x^{m-2r+1}\right]_{x_i-\frac{\Delta x_i}{2}}^{x_i+\frac{\Delta x_i}{2}},$$

$$\int_{y_j-\frac{\Delta y_j}{2}}^{y_j+\frac{\Delta y_j}{2}} P_n ydy = \sum_{s=0}^{D(n)} B_{sn} \left[y^{n-2s+1}\right]_{y_j-\frac{\Delta y_j}{2}}^{y_j+\frac{\Delta y_j}{2}}, \quad (12)$$

where

$$B_{kn} = \frac{(-1)^k (2n-2k)!}{2^n k!(n-k)!(n-2k+1)!}. \quad (13)$$

Using (12), the set of Legendre moments can be computed exactly without loss of information due to sampling. In computing $\{B_{kn}\}$, the factorials can be avoided by utilizing the following recurrence relation:

$$B_{kn} = -\frac{(n-k+1)(n-2k+3)(n-2k+2)}{(2n-2k+2)(2n-2k+1)k} B_{k-1,n} \quad (14)$$

with

$$B_{0,n} = \frac{(2n)!}{2^n n!(n+1)!} = \frac{(2n-1)}{(n+1)} B_{0,n-1},\ B_{0,0} = 1. \quad (15)$$

For the sake of simplicity, we let:

$$Q_n(z_i) = \frac{2n+1}{2} \sum_{k=0}^{D(n)} B_{kn} Z_{i,n-2k+1},\ \ Z_{ip} = [z^p]_{z_i-\frac{\Delta z_i}{2}}^{z_i+\frac{\Delta z_i}{2}}. \quad (16)$$

Notice that $Q_n(z_i)$ is independent of the image and can always be precomputed, stored, and recalled later to avoid repetitive computation. The set of Legendre moment can thus be computed exactly by:

$$\lambda_{mn} = \sum_{i=0}^{M-1} \sum_{j=0}^{N-1} f(x_i, y_j) Q_m(x_i) Q_n(y_j). \quad (17)$$

We name the moments computed by using (17) the exact Legendre moments (ELM), as opposed to the approximated Legendre moments in (10). For computer images, very often the intervals Δx_i and Δy_j are fixed at a constant value. In order to compute the Legendre moments of an discrete-space image $f(i,j)$, $i = 0, 1, \ldots, M-1$, $j = 0, 1, \ldots, N-1$, the image has to be mapped inside the square $[-1, 1] \times [-1, 1]$. We denote the mapped image $f(x_i, y_j) = f(i, j)$ with

$$x_i = -1 + (i+1/2) \times \Delta x, \quad y_j = -1 + (j+1/2) \times \Delta y, \quad (18)$$

and $\Delta x_i = \Delta x = 2/M; \forall i,\ \Delta y_j = \Delta y = 2/N; \forall j$.

4.1 Relationship with Geometric Moments

The geometric moments of order $(m+n)$ is defined as:

$$M_{mn} = \int_{-1}^{1} \int_{-1}^{1} x^m y^n f(x, y) dx dy. \quad (19)$$

If the image is defined only for a discrete set of points (x_i, y_j), we have:

$$M_{mn} = \sum_{i=0}^{M-1} \sum_{j=0}^{N-1} f(x_i, y_j) \int_{x_i-\frac{\Delta x_i}{2}}^{x_i+\frac{\Delta x_i}{2}} \int_{y_j-\frac{\Delta y_j}{2}}^{y_j+\frac{\Delta y_j}{2}} x^m y^n dx dy$$

$$= \frac{1}{(m+1)(n+1)} \sum_{i=0}^{M-1} \sum_{j=0}^{N-1} f(x_i, y_j) Z_{i,m+1} Z_{j,n+1}, \quad (20)$$

where Z_{ip} is defined in (16). Note that there is no approximation involved in (20), so we name the moments as the exact geometric moments. The Legendre moments and the geometric moments are related by:

$$\lambda_{mn} = \frac{(2m+1)(2n+1)}{4} \sum_{r=0}^{D(m)} \sum_{s=0}^{D(n)} B'_{rm} B'_{sn} M_{m-2r,n-2s}, \quad (21)$$

where $B'_{rm} = (m-2r+1)B_{rm}$ and $B'_{sn} = (n-2s+1)B_{sm}$. Hence, the exact Legendre moments can be computed indirectly from the exact geometric moments.

4.2 A Matrix Formulation of the Algorithm

Equation (17) can be written in matrix form as: $\mathbf{M} = \mathbf{Q_y F Q_x^T}$, where $(\cdot)^T$ is the transpose, $\mathbf{M}^T = \{\lambda_{ij}\}_{ij}$, $\mathbf{Q_x} = \{Q_i(x_j)\}_{ij}$, $\mathbf{Q_y} = \{Q_i(y_j)\}_{ij}$, and $\mathbf{F}^T = \{f(x_i, y_j)\}_{ij}$. The matrices $\mathbf{Q_x}$ and $\mathbf{Q_y}$ are computed once and then stored for subsequent calculations of the moments. The matrix form of representation is particular useful in software packages such as MATLAB.

5 EXPERIMENTAL STUDIES

In this section, empirical supports are given for the theoretical framework discussed in previous sections. The performance for the proposed method is evaluated. The results shown are divided into three main sections. In the first section, comparisons are made with theoretical values to verify that the proposed method indeed give exact results. The images used are artificially generated and are deliberately made relatively small in size so that hand calculations can be employed to obtain the theoretical values. In the second section, the image reconstruction aspect is considered. Comparisons are made with both randomly generated images and real images. In the third section, comparisons of computation times between the proposed method and other methods are provided.

5.1 Artificial Images

In this section, artificial images are used so that hand calculations can be employed and the theoretical values can be obtained. This is to verify that the proposed method gives exact values as claimed.

5.1.1 Artifical Image I

For $f(i, j) = K$, $K = \text{constant}$, $\forall(i, j)$, it should be evident that all Legendre moments should give the value of zero, except for λ_{00}. This can be shown by using (1), (4) and the fact that $P_0(x) = P_0(y) = 1$ and $K = KP_0(x) = KP_0(y)$:

$$\lambda_{mn} = \frac{(2m+1)(2n+1)}{4} \int_{-1}^{1} \int_{-1}^{1} P_m(x) P_n(y) K dx dy = K\delta_{m,0}\delta_{n,0}, \quad (22)$$

where $\delta_{k,l}$ is the Kronecker delta. For $K = 1$, the results for exact Legendre moments (ELM, λ_{mn}, (17)), the approximated version using zeroth-order approximation (ZOA, $\hat{\lambda}_{mn}$, (10)) and alternative extended Simpson's rule (AESR, $\hat{\lambda}_{mn}^S$, five dimensional cubature formula II in [9]) are shown in Table 1. We deliberately use a small image of size $M \times N = 8 \times 8$ so that the error due to approximation can be more readily observed. It can be seen that the values given by ELM match the theoretical values while the other methods do not. The error measure

$$\epsilon_{\text{deviation}} = \sum_{m=1}^{L} \sum_{n=0}^{m} \lambda_{m-n,n}^2 \quad (23)$$

can be used to measure the deviation of the moments from zero. The results are shown in Fig. 2. Note that the results for ELM are not shown because $\epsilon_{\text{deviation}} = 0$ for all cases of ELM and, hence, $log_{10}(\epsilon_{\text{deviation}}) = -\infty$.

TABLE 1
Comparison of ELM, λ_{mn}, ZOA, $\widehat{\lambda}_{mn}$ and AESR, $\widehat{\lambda}_{mn}^{\mathrm{S}}$, for $f(i,j) = K = 1$

	ELM, λ_{mn}				ZOA, $\widehat{\lambda}_{mn}$				AESR, $\widehat{\lambda}_{mn}^{\mathrm{S}}$			
	$m=0$	1	2	3	0	1	2	3	0	1	2	3
$n=0$	1	0	0	0	1.0000	0	-0.0391	0	1.0000	0	0.0391	0
1	0	0	0	0	0	0	0	0	0	0	0	0
2	0	0	0	0	-0.0391	0	0.0015	0	0.0391	0	-0.0046	0
3	0	0	0	0	0	0	0	0	0	0	0	0

5.1.2 Artificial Image II

We generate an artificial image $f(i,j) = C_{ij}$, where $\{C_{ij}\} = \mathbf{C}$ and $\mathbf{C}^{\mathrm{T}} = [8\,2\,2\,7; 4\,9\,5\,4; 6\,6\,9\,6; 7\,6\,3\,7]$. The results are shown in Table 2. It can be observed that the values given by ELM (Table 2b) match the theoretical values (Table 2a) while that of ZOA (Table 2c) and AESR (Table 2d) deviates from the theoretical values especially when the order increases.

5.2 Image Reconstruction

The comparison of performance of image reconstruction using the approximated and exact Legendre moments is shown in this experiment. Results for both artificial images and real images are shown.

5.2.1 Random Images

For the sake of fairness, we used randomly generated images for this experiment. First, we generate the image by:

$$f(i,j) = \mathrm{random}(M,N), \quad 0 \le f(i,j) \le 1, \ \forall i,j. \tag{24}$$

We set the size of the image to $M = N = 64$ and by scaling this image, images of different sizes, i.e., 32, 16, and 8, are generated. We then reconstruct these images by using both approximated and exact Legendre moments, up to the maximum order of $m + n \le L = 10, 11, \dots, 40$. The difference between the original image $f(i,j)$ and the reconstruction image $\hat{f}(i,j;L)$ is measured using error function:

$$\epsilon = \frac{1}{MN} \sum_{i=0}^{M-1} \sum_{j=0}^{N-1} \left[\hat{f}(i,j;L) - f(i,j)\right]^2. \tag{25}$$
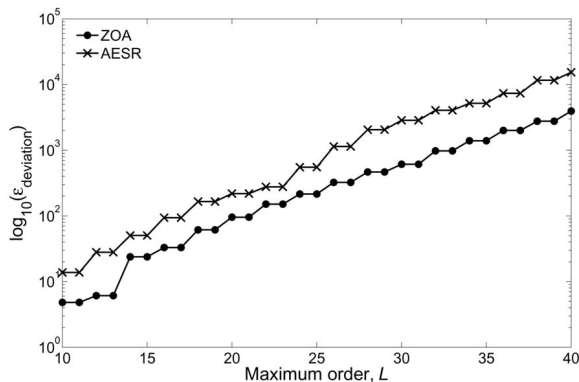

Fig. 2. The logarithmic values of $\epsilon_{\mathrm{deviation}}$ for ZOA and AESR. The values of ELM are not shown because, for all cases of ELM, $\epsilon_{\mathrm{deviation}} = 0$ and, hence, $log_{10}(\epsilon_{\mathrm{deviation}}) = -\infty$.

This process is repeated 50 times and the average results are shown in Fig. 3. It can be seen that, for images of different sizes, the exact Legendre moments consistently give lesser reconstruction errors when compared to approximated Legendre moments. The reconstruction error pertaining to that of exact Legendre moments is steadily decreasing while that of ZOA and AESR begin to increase when the maximum order, L, of the moments is increased up to a certain value. This observation can be explained by using Parseval's theorem. From Parseval's theorem and (8), we know that:

$$E(\hat{f};L) = \int_{-1}^{1} \int_{-1}^{1} \left[\hat{f}(x,y) - f(x,y)\right]^2 dx dy = \epsilon_{\mathrm{moments}} + \epsilon_{\mathrm{approximation}},$$

$$\tag{26}$$

where the two error components, $\epsilon_{\mathrm{moments}}$ and $\epsilon_{\mathrm{approximation}}$, are defined as:

$$\epsilon_{\mathrm{moments}} = \sum_{m=L+1}^{\infty} \sum_{n=0}^{m} \frac{4\lambda_{n,m-n}^2}{[2m+1][2(m-n)+1]},$$

$$\epsilon_{\mathrm{approximation}} = \sum_{m=0}^{L} \sum_{n=0}^{m} \frac{4(\lambda_{n,m-n} - \widehat{\lambda}_{n,m-n})^2}{[2n+1][2(m-n)+1]}. \tag{27}$$

The error $\epsilon_{\mathrm{moments}}$ is due to the information loss as moments with order $m + n > L$ are left out in the reconstruction. It decreases when the number of moments used in the reconstruction is increased, that is, when the values of L is increased. The approximation error is denoted by $\epsilon_{\mathrm{approximation}}$. As opposed to $\epsilon_{\mathrm{moments}}$, it increases when L is increased.

When the low order moments are used for reconstructing the image, the approximation error $\epsilon_{\mathrm{approximation}}$ is small and negligible. Therefore, as we progressively increase the number of moments $\epsilon_{\mathrm{moments}}$ decreases and while the increase of $\epsilon_{\mathrm{approximation}}$ is negligible, the overall error $E(\hat{f};L)$ of the reconstructed image decreases. But, as more moments are included in the reconstruction process, $\epsilon_{\mathrm{approximation}}$ increases up to a certain value and are no longer negligible, so much so that its effect overcomes that of $\epsilon_{\mathrm{moments}}$. In this case, including more moments in the reconstruction process will not decrease but, instead, increase the error of the reconstructed image, as is shown in Fig. 3. It can be seen that this problem is solved by using the exact Legendre moments where $\epsilon_{\mathrm{approximation}} = 0$.

5.2.2 Real Images

Real images, shown in Fig. 4, are also used as test images. The average reconstruction results for the eight images are shown in Fig. 5. In all cases, the ELM outperforms all the other methods.

TABLE 2
Comparison of ELM, λ_{mn}, ZOA, $\widehat{\lambda}_{mn}$ and AESR, $\widehat{\lambda}^{\mathrm{S}}_{mn}$, with the Theoretical Values

Theoretical	$m = 0$	1	2	3
$n = 0$	5.6875	-0.3281	0.8203	0.4990
1	0.7969	0.2461	-1.3184	0.2410
2	-0.8203	-0.4395	5.4932	0.4486
3	-0.5674	-0.6819	-0.9613	2.0240

ELM, λ_{mn}	$m = 0$	1	2	3
$n = 0$	5.6875	-0.3281	0.8203	0.4990
1	0.7969	0.2461	-1.3184	0.2410
2	-0.8203	-0.4395	5.4932	0.4486
3	-0.5674	-0.6819	-0.9613	2.0240

ZOA, $\widehat{\lambda}_{mn}$	$m = 0$	1	2	3
$n = 0$	5.6875	-0.3281	-0.0684	0.6187
1	0.7969	0.2461	-1.4429	0.1512
2	-1.7090	-0.3882	5.6320	0.5122
3	-0.8579	-0.7716	-0.3466	2.2174

AESR, $\widehat{\lambda}^{\mathrm{S}}_{mn}$	$m = 0$	1	2	3
$n = 0$	5.6875	-0.3281	1.7090	0.3794
1	0.7969	0.2461	-1.1938	0.3307
2	0.0684	-0.4907	5.0766	0.4224
3	-0.2769	-0.5922	-1.6668	1.7651

5.2.3 Block Encoding

We divide the images in Fig. 4 in blocks of 8×8, compute the Legendre moments of each block up to order $L = 0, 1, 2, \ldots, 10$, and then reconstruct the blocks from the computed set of moments. The error of the reconstructed image when compared to the original image is computed using (25). The average results for all the images in Fig. 4 are shown in Fig. 6.

5.3 Computation Time

5.3.1 Computation Time of the Moment Kernels

Basically, the computation of Legendre moments involve two steps. In the first step, the moment kernels are generated. The kernels for the ELM and ZOA are $P_n(x_i)$ and $Q_n(x_i)$, respectively. As for AESR, if the dimension of the cubature formula used is dim, then the computations involved is approximately dim times that of
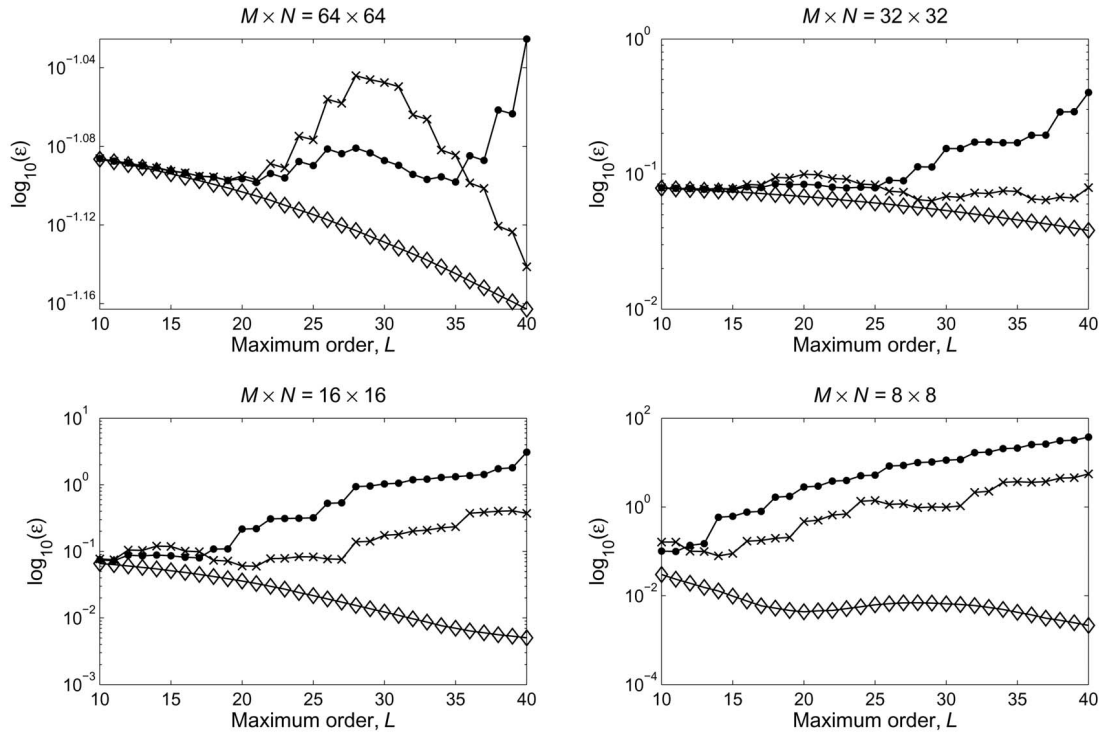

Fig. 3. Logarithmic values of reconstruction errors ϵ for images of different sizes using ELM, ZOA, and AESR. $m + n \leq L$.
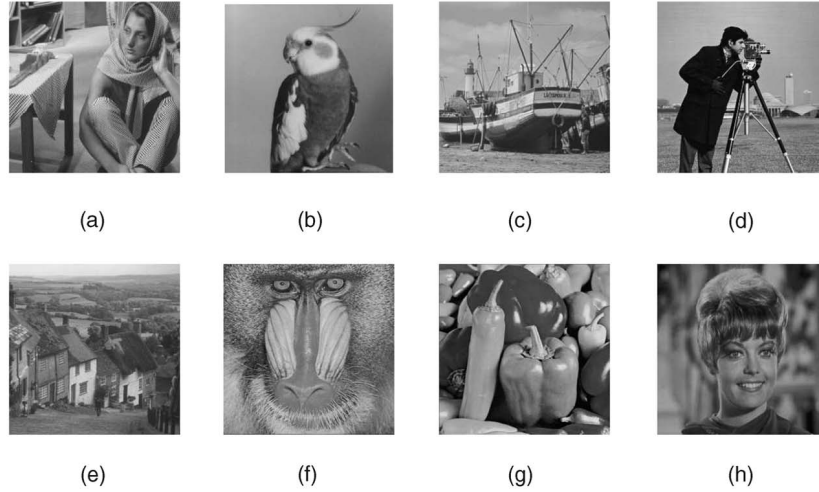
Fig. 4. Real images. $M \times N = 128 \times 128$. (a) Barb. (b) Bird. (c) Boat. (d) Cameraman. (e) Goldhill. (f) Mandrill. (g) Peppers. (h) Zelda.

ZOA. Since the moment kernels are independent of the image, they can be computed in advance, stored, and retrieved whenever necessary. In the second step, the moment kernels are multiplied with the image function and results in the set of Legendre moments. In this particular step, the numbers of operations in this step for both ZOA and ELM are identical, that is, for an image with $M \times N$ pixels, MN multiplications and $MN - 1$ additions are involved.

The computation complexity of Legendre moments are crucial for real-time application. Table 3 shows the computation time[1] of the moment kernels. Note that the table is obtain by generating 1,000 polynomial points, i.e., $i = 0, 1, \ldots, 999$, and the values of the computation time taken to generate the kernels are averaged over 100 trials. We used the recurrence relation (5) to generate $P_n(x_i)$ and $Q_n(x_i)$ is generated using equations (14)-(16). It can be seen that, although the computation time of the kernel of the ELM, $Q_n(x_i)$, is longer when compared to that of the ZOA, $P_n(x_i)$, the differences are still relatively small and, hence, the implementation of the ELM in real-time application is feasible and inexpensive in terms of computation complexity. Furthermore, as mentioned above, these kernels are independent of the image and they can always be stored in advance to avoid repetitive computation and recalled whenever necessary. In this case, the computation times for both the conventional and proposed methods are identical.

5.3.2 Comparison of the Proposed Method with the Indirect Method Using Geometric Moments

Though the exact values can be obtained using geometric moments, the computation time to involved is much longer than the proposed method. In this experiment, we make a comparison between the computation time of (17) and (21), i.e., the direct method by using $Q_n(x_i)$ and the indirect method by using the set of geometric moments. For this purpose, the "Cameraman" image in Fig. 4 is used as our test image and the Legendre moments up to order $m_{\max} = n_{\max} = C$, $C = 10, 20, \ldots, 40$ are calculated. This process is repeated for 100 times and the average values for the computation time are then taken. The results of both methods are shown in Table 4. It is evident that the proposed method shows improvement over the indirect method in terms of computation time.

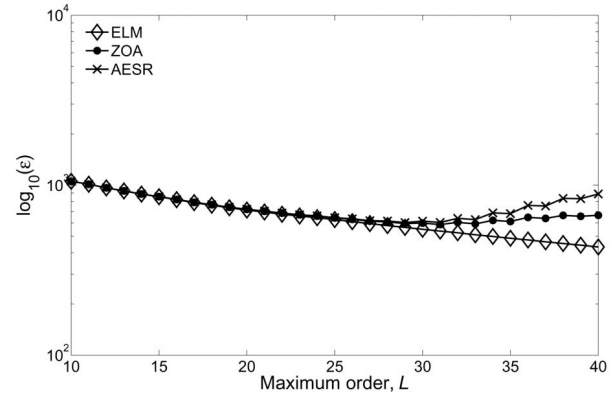1. All computations are done with Matlab running on a 2.8GHz PC with 512MB RAM.

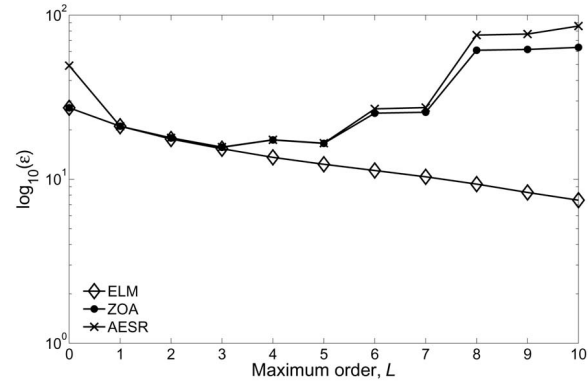Fig. 5. Average reconstruction error for the images in Fig. 4.

Fig. 6. Average block encoding error.

TABLE 3
Comparison of Average Computation Time (ms) for the Kernel of ELM, ZOA, and AESR Up to Order n_{max}

$n_{\max}$	10	20	30	40
ELM	4.06	9.21	11.72	24.37
ZOA	3.28	6.57	9.22	12.82
AESR	20.40	40.86	61.95	82.97

TABLE 4
Comparison of Average Computation Time (ms) for the Proposed
Method and the Indirect Method Using Geometric Moments to Generate
Legendre Moments Up to Order $m_{\max} = n_{\max} = C$

C	10	20	30	40
Proposed	2.03	2.81	4.22	5.31
Using Geometric Moments	6.56	23.60	50.32	88.75

6 CONCLUSION

This paper proposes a method for the exact computation of the set of Legendre moments. It is shown that zeroth-order approximation and alternative extended Simpson's rule cause error in the corresponding Legendre moments, especially when the order is high. Legendre moments calculated using proposed method show exactly the same values when compared to those obtained by theoretical calculations. The results of image reconstruction from the exact Legendre moments also show improvement over that of the approximated Legendre moments. Particularly, when the high order Legendre moments are used, the approximation methods progressively show an increase in the reconstruction error. This is undesirable and we show the problem can be remedied by using the proposed method. Using the proposed method, the reconstruction error decreases steadily when the order of the moments is increased. It is also shown that the computation time difference between the proposed method and the conventional method can be eliminated by first storing the moment kernels.

ACKNOWLEDGMENTS

REFERENCES

[1] M. Teague, "Image Analysis Via the General Theory of Moments," *J. Optical Soc. Am.,* vol. 70, pp. 920-930, Aug. 1980.
[2] C.-W. Chong, R. Paramesran, and R. Mukundan, "Translation and Scale Invariants of Legendre Moments," *Pattern Recognition,* vol. 37, no. 1, pp. 119-129, 2004.
[3] M. Mandal, T. Aboulnasr, and S. Panchanathan, "Image Indexing Using Moments and Wavelets," *Proc. Int'l Conf. Consumer Electronics, Digest of Technical Papers,* pp. 557-565, June 1996.
[4] J. Haddadnia, K. Faez, and P. Moallem, "Neural Network Based Face Recognition with Moment Invariants," *Proc. Int'l Conf. Image Processing,* vol. 1, pp. 1018-1021, Oct. 2001.
[5] H. Qjidaa and L. Radouane, "Robust Line Fitting in a Noisy Image by the Method of Moments," *IEEE Trans. Pattern Analysis and Machine Intelligence,* vol. 21, no. 11, pp. 1216-1223, Nov. 1999.
[6] R. Koekoek and R. Swarttouw, "The Askey-Scheme of Hypergeometric Orthogonal Polynomials and Its Q-Analogue," Faculty of Technical Math. and Informatics Report 98-17, Delft, Netherlands: Technische Univ. Delft, pp. 46-47, 1998.
[7] A. Erdelyi, V. Magnus, F. Oberhettinger, and F. Tricomi, *Higher Transcendental Functions.* McGraw Hill, 1953.
[8] G. Szegö, *Orthogonal Polynomials.* New York: Am. Math. Soc., 1939.
[9] S. Liao, "Image Analysis by Moments," PhD dissertation, Univ. of Manitoba, Winnipeg, Canada, 1993.
[10] S. Liao and M. Pawlak, "On Image Analysis by Moments," *IEEE Trans. Pattern Analysis and Machine Intelligence,* vol. 18, no. 3, pp. 254-266, Mar. 1996.
[11] S.X. Liao and M. Pawlak, "On the Accuracy of Zernike Moments for Image Analysis," *IEEE Trans. Pattern Analysis and Machine Intelligence,* vol. 20, no. 12, Dec. 1998.
[12] J.D. Zhou, H.Z. Shu, L.M. Luo, and W.X. Yu, "Two New Algorithms for Efficient Computation of Legendre Moments," *Pattern Recognition,* vol. 35, no. 5, pp. 1143-1152, May 2002.
[13] H.Z. Shu, L.M. Luo, W.X. Yu, and J.D. Zhou, "Fast Computation of Legendre Moments of Polyhedra," *Pattern Recognition,* vol. 34, no. 5, pp. 1119-1126, May 2001.
[14] H.Z. Shu, L.M. Luo, W.X. Yu, and Y. Fu, "A New Fast Method for Computing Legendre Moments," *Pattern Recognition,* vol. 33, no. 2, pp. 341-348, Feb. 2000.
[15] R. Mukundan and K. Ramakrishnan, "Fast Computation of Legendre and Zernike Moments," *Pattern Recognition,* vol. 28, no. 9, pp. 1433-1442, 1995.
[16] R. Mukundan and K.R. Ramakrishnan, *Moment Functions in Image Analysis.* Singapore: World Scientific Publishing, 1998.
[17] J. Shen and D. Shen, "Orthogonal Legendre Moments and Their Calculation," *Proc. 13th Int'l Conf. Pattern Recognition,* pp. 241-245, 1996.
[18] C. Teh and R. Chin, "On Image Analysis by the Method of Moments," *IEEE Trans. Pattern Analysis and Machine Intelligence,* vol. 10, no. 4, pp. 496-513, 1988.
[19] E. Kreyszig, *Advanced Engineering Mathematics,* sixth ed. John Wiley and Sons, 1988.

▷ **For more information on this or any other computing topic, please visit our Digital Library at** www.computer.org/publications/dlib.